AIP | Review of Scientific Instruments

Design of a self-aligned, wide temperature range (300 mK-300 K) atomic force microscope/magnetic force microscope with 10 nm magnetic force microscope resolution

Özgür Karc, Münir Dede, and Ahmet Oral

Citation: Review of Scientific Instruments **85**, 103705 (2014); doi: 10.1063/1.4897147
View online: http://dx.doi.org/10.1063/1.4897147
View Table of Contents: http://scitation.aip.org/content/aip/journal/rsi/85/10?ver=pdfcov
Published by the AIP Publishing

Design of a self-aligned, wide temperature range (300 mK-300 K) atomic force microscope/magnetic force microscope with 10 nm magnetic force microscope resolution

Özgür Karcı,[1,2] Münir Dede,[1] and Ahmet Oral[3,a)]
[1]*NanoMagnetics Instruments Ltd., Hacettepe - İvedik OSB Teknokent, 1368. Cad., No: 61/33, 06370, Yenimahalle, Ankara, Turkey*
[2]*Department of Nanotechnology and Nanomedicine, Hacettepe University, Beytepe, 06800 Ankara, Turkey*
[3]*Department of Physics, Middle East Technical University, 06800 Ankara, Turkey*

(Received 21 May 2014; accepted 21 September 2014; published online 7 October 2014)

We describe the design of a wide temperature range (300 mK-300 K) atomic force microscope/magnetic force microscope with a self-aligned fibre-cantilever mechanism. An alignment chip with alignment groves and a special mechanical design are used to eliminate tedious and time consuming fibre-cantilever alignment procedure for the entire temperature range. A low noise, Michelson fibre interferometer was integrated into the system for measuring deflection of the cantilever. The spectral noise density of the system was measured to be ∼12 fm/$\sqrt{}$Hz at 4.2 K at 3 mW incident optical power. Abrikosov vortices in BSCCO(2212) single crystal sample and a high density hard disk sample were imaged at 10 nm resolution to demonstrate the performance of the system.
 [http://dx.doi.org/10.1063/1.4897147]

I. INTRODUCTION

Invention of atomic force microscopy[1] (AFM) has revolutionized the surface science. AFM also enabled the scientists to measure variety of forces between the tip and sample, like magnetic and electric forces. Measurement of magnetic forces using force microscopy has opened a new avenue in magnetic imaging.[2] Furthermore, magnetic force microscope (MFM) is a relatively simple and easy to use and can be operated in a wide range of environments like vacuum, high magnetic fields, low temperatures, etc. in contrast to the other magnetic imaging techniques. Magnetic imaging at variable temperatures and external high magnetic field has special importance in material science and physics like vortex imaging[3–7] or manipulation of vortices[8,9] in superconductors, magnetic phase separation,[10,11] domain walls in ferromagnetic thin films,[12,13] magnetization reversal,[14] and topological insulators.[15] Applications of the low temperature MFM on various material systems were discussed extensively in the literature,[16–18] too.

There is relatively limited number of low temperature AFM & MFM (LT-MFM) described in the literature[19–24] at temperatures at and below 4 K. Since the space is quite limited to a few centimeters, measuring deflection of the cantilever in a cryostat is not simple like in the ambient systems. A number of different deflection measurement methods are reported by various groups. Most of the optical methods rely on the fibre interferometer,[19] however due to thermal contractions the cantilever should be aligned with respect to the fibre. Other methods are self-sensing methods which require no optical alignment. These utilize piezoresistive cantilevers[4,25] and quartz tuning forks with a magnetic tip glued at the end of one of the prongs.[26] However, the sensitivity of the piezoresistive sensors is limited because of the power dissipation[25] and the spring constant of the quartz tuning is too high, ∼1800 N/m, which limits the magnetic sensitivity and applicability. Furthermore, only a few designs[27,28] were reported for LT-MFM below 1 K operations for ^{3}He systems.

In this study, we report an ultra low noise, ∼12 fm/$\sqrt{}$Hz, self-aligned Michelson fibre interferometer based LT-AFM/MFM operating between ∼300 mK to 300 K which does not require any optical alignment between fibre and cantilever, capable of achieving ∼10 nm magnetic resolution. We have used an alignment chip from NanoSensors[29] or Applied NanoStructures[30] to make the system alignment free and very easy to operate, compared to other microscopes. The cantilevers suitable for these alignment chips, which can be purchased off the shelf from these manufacturers, have groves matching the protrusions on the chip, enabling us to locate the end of fibre with respect to the cantilever with ±3 μm accuracy in XYZ directions when a new cantilever is mounted. The mechanical design of the LT-AFM/MFM was carefully crafted and tuned such that the thermal contractions are cancelled out and minimized during the temperature cycling, enabling us hassle free operation, down to ∼300 mK. Therefore, all the tedious alignment procedures and unnecessary positioning mechanisms which would complicate the design were eliminated for a LT-AFM/MFM system. The microscope is very easy to operate, similar to an ambient AFM/MFM system.

II. MICROSCOPE DESIGN

A. Microscope head

We designed the microscope head with 23.6 mm OD and 200 mm length to fit into a 27 mm free ID sample space of ^{3}He cryostat (Oxford Instruments, Heliox TL) as well as standard helium cryostats from various manufacturers. The microscope

a)Author to whom correspondence should be addressed. Electronic mail: orahmet@metu.edu.tr

head is detachable using a docking station, comprising low temperature high density miniature connectors, which makes it possible to attach the microscope to many different cryostat systems. Microscope head is composed of two concentric piezotubes: the inner piezo tube is used for scanning and the outer one is used for the sample positioner. The length of the scan piezo is 3″ and has ∼18 μm XY scan range and ∼1.4 μm Z range at 4 K. The scan piezo is composed of quadrant electrodes and a dither piezo at the end, which is used to dither the cantilever for dynamic mode operation. Concentric design eliminates most of the thermal drift. The optical fibre is also connected using an FC-APC type angle polished single mode fibre connector to minimize the reflection located somewhere between 300 K-300 mK for ease of removal of the LT-AFM/MFM.

The length of the sample slider piezo is 1.5″, which also has quadrant electrodes and a glass tube mounted at the end. A sample slider puck is loaded on this glass tube using a leaf spring and two screws. The stick-slip sample approach mechanism is used to move the sample in XYZ directions. Sample slider piezo can move the sample in z direction ∼10 mm and in XY directions within Ø3 mm. We have also integrated a capacitive encoder to measure the XY position with ±3 μm accuracy, with no heat dissipation. The motion and step sizes 50-800 nm are controlled by our dedicated LT-AFM/MFM Control Electronics and software from NanoMagnetics Instruments Ltd.

B. Microscope inserts

Two separate inserts were designed for the microscope head. One for standard helium cryostat and the second one were for an Oxford Instruments ^{3}He cryostat, Heliox TL. The first insert is a simple stick with radiation baffles, fiber connector holder, and a three connector docking station. The length of the stick is adjusted with respect to the magnet center and the radiation shields are placed along the body. This design provides us flexibility to use the microscope for any other cryostats.

The second insert for the ^{3}He cryostat is designed to minimize heat load to the microscope as shown in Fig. 1(a). The insert has two stages: 4 K and 1 K pot. They are made of high purity copper and are in a physical contact with the variable temperature insert (VTI) of the cryostat. Constantan ribbon cable was chosen to minimize the heat load. The ribbon cables are tightly wound on the copper posts at the both 4 K and 1 K pots for thermally anchoring the heat load as shown in Fig. 1(b). The microscope docking station is attached just beneath 4 K pot. The microscope head attached to the 1 K pot by using a thin walled stainless steel tubing and G10 Helium displacer to minimize the heat load into the ^{3}He liquid.

C. Self-aligned holder design

We designed the LT-AFM/MFM head with a self-aligned cantilever holder mechanism which keeps the XYZ position of the cantilever with respect to fibre within ± 6 μm accuracy, as we change the temperature from 300 K to 300 mK. An alignment chip (from NanoSensors or Applied Nanostructures) is mounted under the cantilever. There are three protrusions on the chip and three matching groves at the back of the cantilevers. When a new cantilever is placed on this alignment chip, ±3 μm repositioning accuracy is obtained. The cantilever alignment chip is glued on top of a small piezo stack element and this assembly is aligned with respect to the cleaved fibre end under the optical microscope before everything is glued using a low temperature compatible epoxy. The separation between the back of the cantilever and fibre is arranged to be ∼30 μm, which is a secure gap distance for cantilever replacement as shown in Fig. 2. The cantilever is kept in position by a metal spring. The whole fibre-cantilever assembly is tilted 11° with respect to the sample. This self-aligned design works very reliably even after many temperature cycles between 300 mK-300 K. Alignment procedures

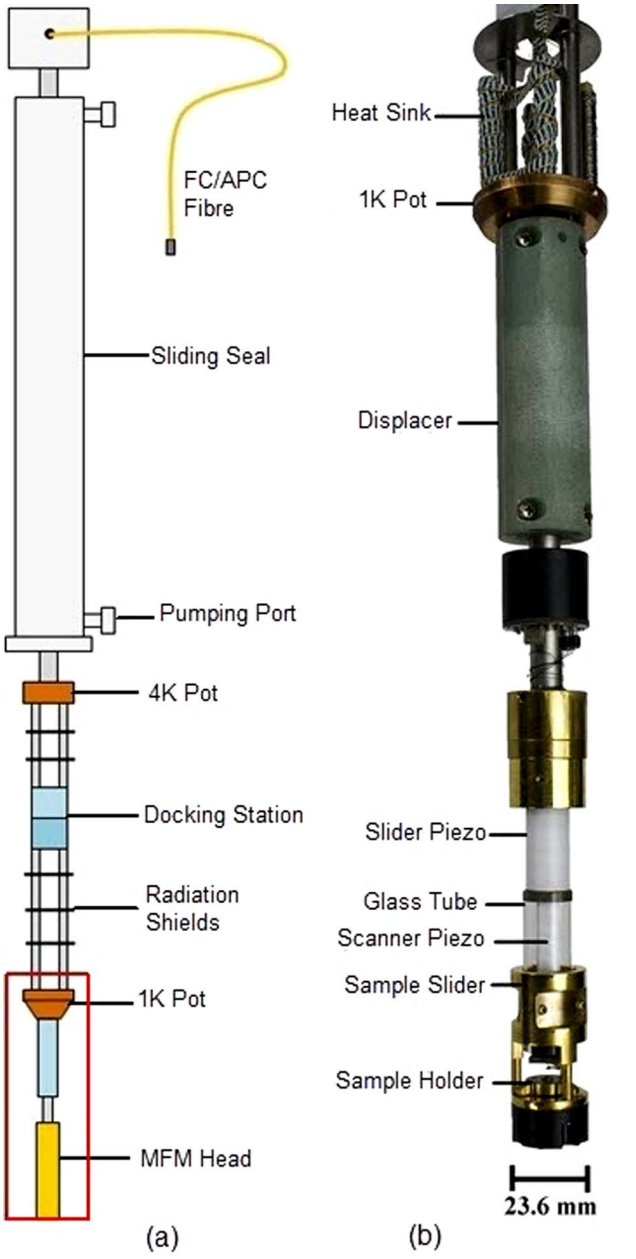

FIG. 1. AFM/MFM head (a) schematic design of the head, (b) photograph of the head.

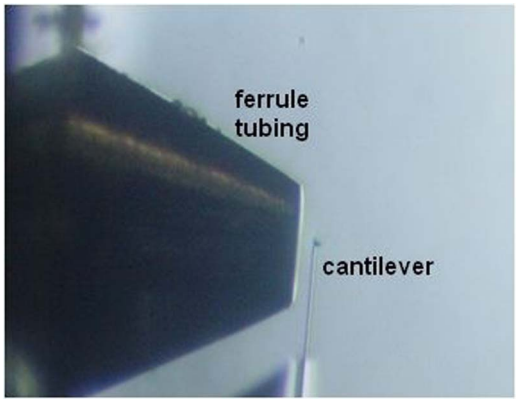

FIG. 2. Alignment photograph of the cantilever with respect to the fibre from side view. Nominal length of the lever is 225 μm.

for the users are eliminated and the usability of the microscopes is greatly improved.

When the microscope was cooled down from 300 K to 300 mK, the thermal contractions in the z-direction could be easily measured, directly by the fibre interferometer. During the cool down process, typically 6 period ($\lambda/2$, $\lambda = 1310$ nm) shifts were measured in the interference pattern, which corresponds to ~3.93 μm displacements in z-direction. The shift is in opposite direction during cooling and warming up process. For the XY drift, a simple calculation is shown below to find the geometric spot size of the laser beam. The core diameter of the fibre is 10 μm with a nominal numerical aperture (N.A.) value of 0.14 and the nominal width of the cantilevers is 28 μm. As shown in Fig. 3, the spot size which falls onto the back of the cantilever is calculated to be 19 μm, for the initial separation of 30 μm. We calculated the typical XY drift to be less than 5 μm for the entire temperature range of 300 K to 300 mK.

III. FIBRE INTERFEROMETER

A low noise Michelson type fibre interferometer is designed for measuring the cantilever displacement. This is similar to Rugar design[31] with a couple of tricks to improve the sensitivity.[32] A pigtailed, 1310 nm laser diode is operated at constant power up to 5 mW and coupled into a 2 × 2, single mode, 50% fibre splitter, as shown in Fig. 4. One of the fibre splitter outputs is connected to the fibre which goes to the end of cantilever into the LT-MFM system. The other output is connected to the pigtailed reference photodiode which is used for monitoring the laser power. The input of fibre splitter is connected to the pigtailed signal photodiode. The end of fibre is cleaved using fibre cleaver. Typically, 3% of the light is reflected back from at the end of cleaved fibre. The remaining light exits the fibre and hits the cantilever and then part of it is reflected back into the fibre. These two light beams pass through the fibre splitter and reaches to signal photodiode where they interfere. This interference generates a photocurrent which can be written as,

$$i = i_0\left[1 - V\cos\left(\frac{4\pi d}{\lambda}\right)\right], \tag{1}$$

where **V**, **d**, and **λ** are visibility, cantilever-fibre separation, and wavelength of the laser, respectively. The interferometer is at the most sensitive position at the quadrature points, d = λ/8, 3λ/8, 5λ/8, . . . ,. The slope of the interference is

$$\frac{\Delta i}{\Delta d} = 4\pi i_0 \frac{\mathrm{V}}{\lambda}, \tag{2}$$

where $\Delta \boldsymbol{d}$ is the displacement of the cantilever. The typical value of the slope for our interferometer is ~4 mV/Å. The quadrature point of the fibre interferometer, where the slope is maximum, is determined by measuring the interference pattern by moving the cantilever with the stack piezo beneath the cantilever. The stack piezo is driven between 0-125 V forward and backward direction, with respect to the fibre. The quadrature point is detected by the software and locked into position during the operation with a subroutine in the software. Injection of RF current into the laser diode, which is crucial to noise reduction, broadens the linewidth and reduces the mode hopping and interference noise from other reflections.

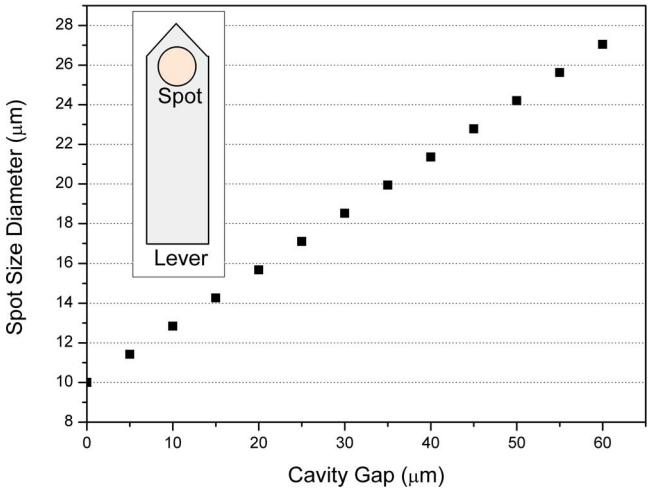

FIG. 3. Spot size versus cavity gap graph. Inset shows the spot on the lever.

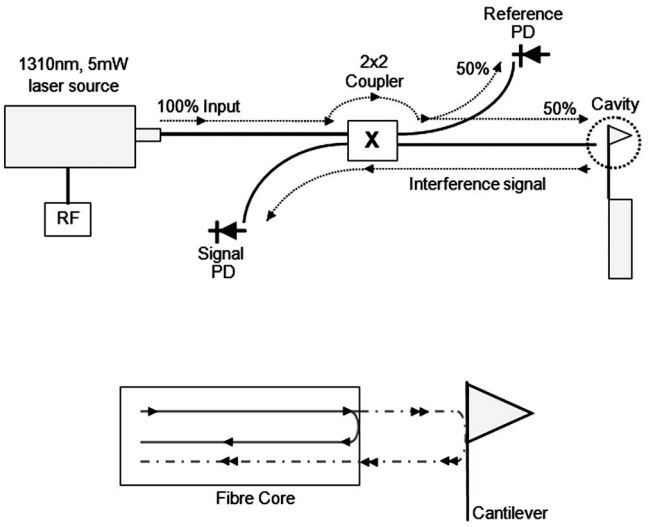

FIG. 4. Schematic design of the Michelson fibre interferometer and the cavity which shows reflections of the laser beams.

IV. EXPERIMENTAL RESULTS

A. Noise measurement

PPP-MFMR cantilevers with 3 N/m nominal stiffness and ∼70 kHz resonant frequency (from NanoSensors Inc.) were used during the experiments. The noise is measured with a Rohde-Schwarz spectrum analyzer and compared with the calculated spectral noise density of the fibre interferometer, as shown in Fig. 5. The noise was measured to be ∼25 fm/$\sqrt{\text{Hz}}$ at 300 K and ∼12 fm/$\sqrt{\text{Hz}}$ at 4 K. The spectral noise density, S, is calculated according to the equation and fitted to the experimental data:[33]

$$S = \sqrt{\left(\frac{2k_B T}{\pi f_0 k Q} \frac{1}{\left(1 - \left(\frac{f}{f_0}\right)^2\right)^2 + \left(\frac{f}{f_0 Q}\right)^2} \right)}, \quad (3)$$

where f_o, f, T, Q, k, and k_B are resonance frequency, frequency, temperature, quality factor, spring constant, and Boltzmann constant, respectively. After the fit the parameters were found to be $f_o = 61\,590$ Hz, $Q \sim 1000$ and $k = 1.5$ N/m. The Shot noise can be calculated according to the equation:

$$\bar{v}_{shot} = \sqrt{2eS_{PD}PR_F}\left(\frac{V}{\sqrt{Hz}}\right), \quad (4)$$

where e, S_{PD}, P, and R_F are electronic charge (1.6×10^{-19} C), responsivity of the photo detector (1A/W), average power falls onto the photo detector (229 μW), and photocurrent passes through resistor of the operational amplifier circuit, respectively. The noise level of our fibre interferometer is observed to be very close to the shot noise limit, which is calculated to be 7.8 fm/$\sqrt{\text{Hz}}$. The shot noise of the interferometer can be decreased further, if the incident power on the photo detector is increased.

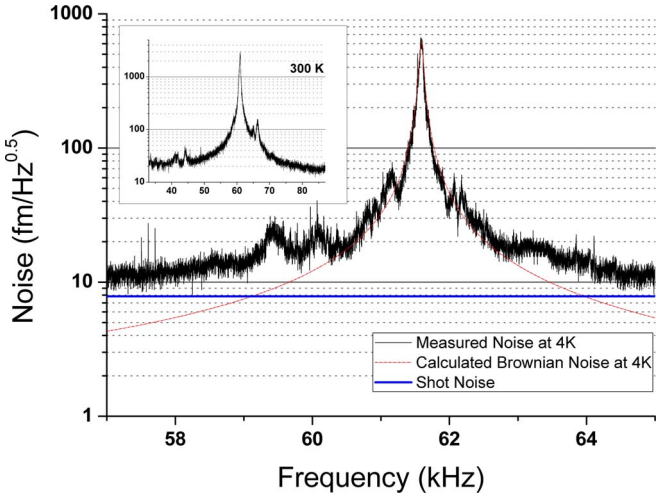

FIG. 5. Measured and calculated spectral noise density at 4.2 K. Inset shows the measured noise at 300 K. The cantilever (PPP-MFMR) has 61 590 Hz resonance frequency and 1.5 N/m calculated spring constant.

B. LT-AFM/MFM imaging

A mica sample was imaged to demonstrate the performance and to observe the atomic terraces. Prior to the experiment, the mica sample was cleaved using scotch tape and etched in 48% HF solution (Merck, Germany) for 4 h. The sample was then washed with deionised water and dried with dry nitrogen. Atomic terraces of mica were imaged (∼10 Å) at various temperatures in tapping mode[34] AFM as shown in Fig. 6. In this mode, the cantilever is oscillated by the dither piezo in its resonance frequency with constant excitation. Oscillation amplitude of the cantilever is used for as the feedback signal. Approximately, half of the free oscillation amplitude is used for feedback set point, which gives good results for imaging most of the time.

The microscope was cooled down by pumping the liquid ^{3}He below 1 K. Without switching on the SPM controller, the system reached 320 mK which confirmed that thermal load was less than cooling power of the cryostat. Even if, when the SPM controller was switched on, without switch on the laser diode of the interferometer, the temperature stayed the same. This showed that there was no power dissipation at both piezos and wiring of the head. When the laser diode was switched on with power of ∼4 mW, the temperature showed sudden rise. However, the temperature was stable around at ∼350 mK with 2 mW laser power and we could image CoPt multilayers, as shown in Fig. 7. The image was acquired in lift-mode MFM. In this mode, the topography of the

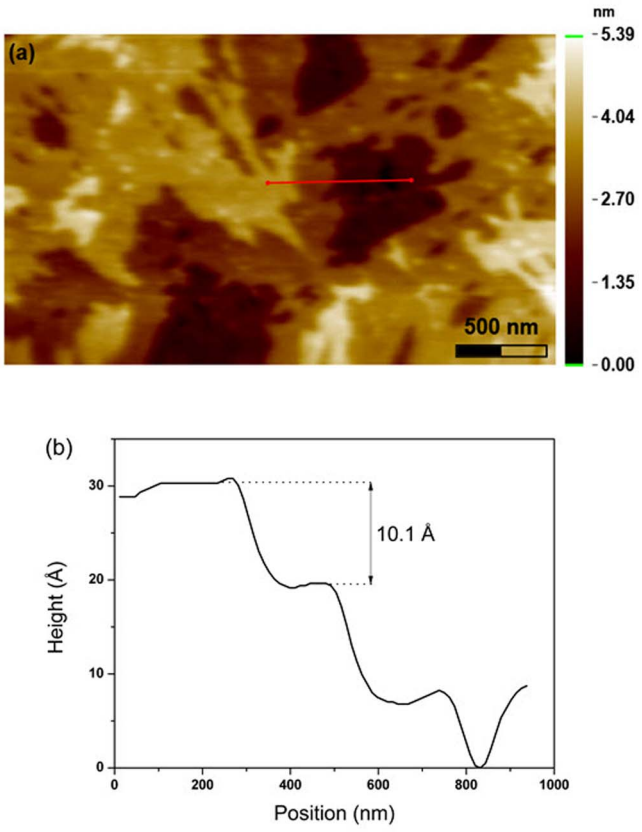

FIG. 6. (a) Tapping mode AFM image on HF etched mica sample recorded at 77 K. (b) The cross-section on the image shows atomic steps. Scan size is 3 μm × 1.75 μm with scan speed of 1 μm/s.

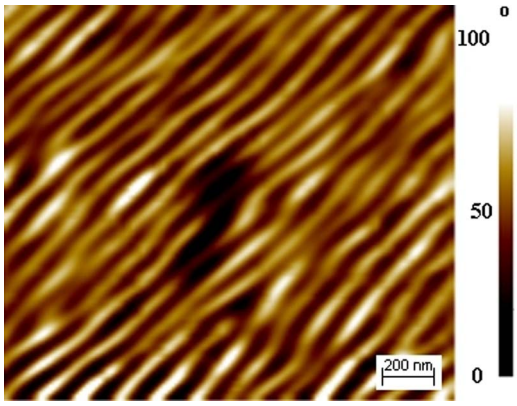

FIG. 7. MFM image shows magnetic domains of the CoPt multilayers at 350 mK. Scan size is 1.6 μm × 1.4 μm with scan speed of 1 μm/s.

sample is recorded during forward scan in tapping mode. Prior to backward scan on the same line, feedback is frozen and the cantilever is lifted by ∼20-100 nm and phase shifts caused by magnetic forces are recorded as an MFM image. The typical oscillation amplitude was 40 nm and lift height was 100 nm.

Abrikosov vortices in BSCCO(2212) single crystal were also imaged at 4.5 K. Prior to the experiment, the sample was cleaved using scotch tape and the cantilever (PPP-MFMR, NanoSensors Inc.) was magnetized in the cryostat at 300 K. The sample was field cooled down to 4.5 K under the magnetic field of +40 Oe that field direction was the same with tip magnetization direction. BSCCO is type-II superconductor and the field was trapped in the vortices as seen in Fig. 8(a). The vortices form perfect hexagonal honeycomb structures in the sample and each vortex carries single flux quantum, Φ_o, which has a value of $\Phi_o = h/2e = 2.07 \times 10^{-15}$

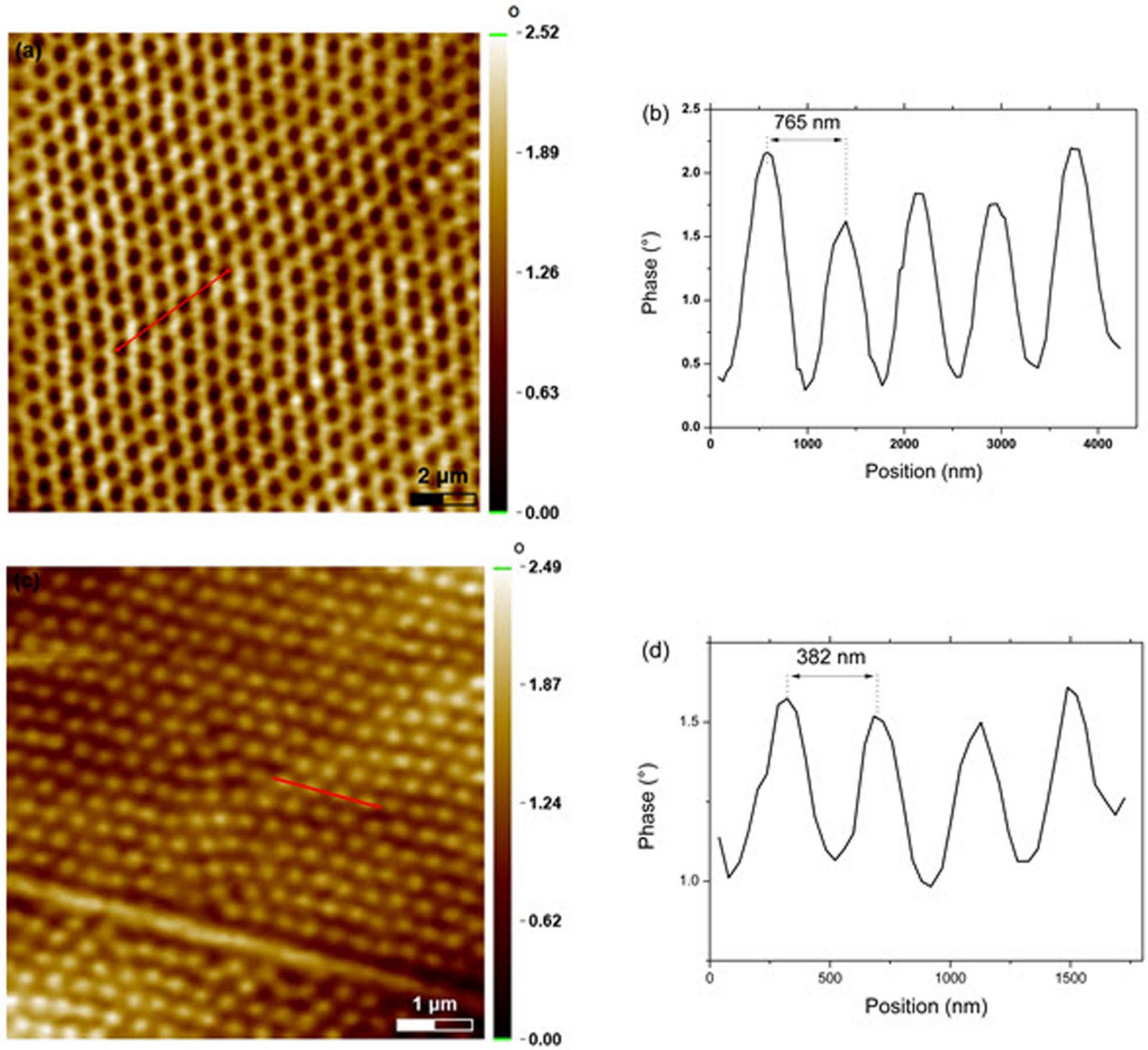

FIG. 8. MFM images of Abrikosov vortices in BSCCO single crystal at 4.5 K. (a) The sample was cooled down under +40 Oe external magnetic field. Scan size is 15 μm × 15 μm with scan speed of 10 μm/s, (b) cross-section on the image (a), (c) the sample was cooled down under −160 Oe external magnetic field. Scan size is 6.7 μm × 6.7 μm with scan speed of 4 μm/s, and (d) cross-section on the image (c). Tip was magnetized in the positive field direction at 300 K.

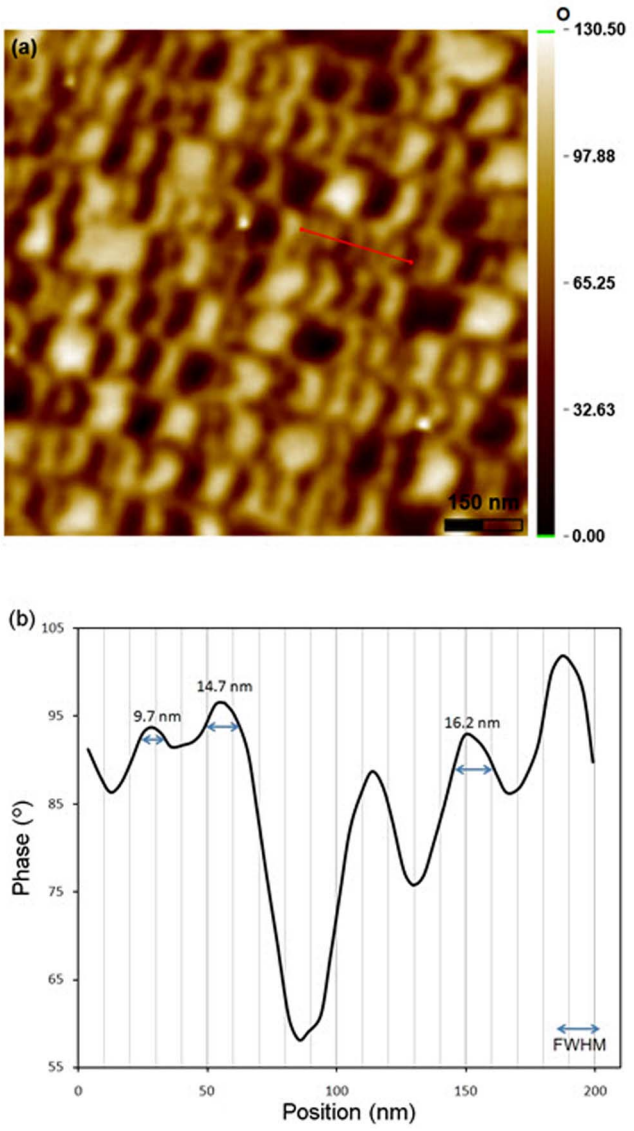

FIG. 9. (a) MFM image of a perpendicular recording medium, Seagate Momentus 5400.6 hard disk with 398 Gbpsi density, at 77 K and (b) a cross-section on the image with full width half maximum (FWHM) analysis.

T m^2. The vortex spacing between two adjacent cores was measured ~765 nm and the phase difference was measured to be ~2° as seen in Fig. 8(b). The vortex spacing, a, can be calculated for a triangular unit cell according to the equation:

$$a = \sqrt{\frac{2\Phi_0}{\sqrt{3}B}}, \quad (5)$$

where B is applied external field for cool down. For our case of +40 Oe applied magnetic field, the vortex spacing calculated to be 773 nm which was compatible with measured value. When the field is increased, the vortices are getting closer and the vortex density is increased. For another experiment, the sample was cooled down in an opposite field of −160 Oe with respect to the tip. The vortex cores appear as bright spots as shown in Fig. 8(c) and getting closer as expected. The average vortex spacing was measured to be ~382 nm as seen in Fig. 8(d) which was also close to calculated value of 387 nm. The slight discrepancy in vortex spacing could be caused by remnant field in the superconducting magnet. In Fig. 8(c), another part of the sample was imaged and it was seen that the vortices were pinned along the atomic terrace of sample since surface defects behave as pinning centers. The images were obtained in constant height mode with 65 nm lift height.

The ultimate performance of the microscope was demonstrated on the high density perpendicular recording media, Seagate Momentus 5400.6 hard disk with 398 Gbpsi as shown in Fig. 9(a) at 77 K in Helium exchange gas. Super sharp cantilevers were used (SSS-MFMR, NanoSensors Inc.) for MFM imaging. Typical oscillation amplitudes between 10 to 15 nm were employed with lift-off amount of 15-30 nm to achieve this resolution. The cross-section on the bit sequence is shown in Fig. 9(b) which routinely gives 10 nm MFM resolution.

V. CONCLUSIONS

We designed and successfully tested a self-aligned, wide temperature range LT-AFM/MFM between 300 mK to 300 K. This self-aligned system eliminates all tedious fibre-cantilever alignment procedure and mechanisms. We achieve 12 fm/$\sqrt{}$Hz noise level and routinely reach 10 nm MFM resolution with off the shelf cantilevers. The noise level and the resolution of the microscope could be further enhanced using a fibre Fabry-Perot interferometers[35,36] with ~1 fm/$\sqrt{}$Hz noise level,[37] which is subject to ongoing research.

ACKNOWLEDGMENTS

The project was partially supported by TÜBİTAK Grant No 111T802. Ö.K. wishes to thank Dr. Olav Helvig from Western Digital, San Jose, California, United States for CoPt multilayers samples and Professor Kazuo Kadowaki, Tsukuba University, Japan for BSCCO samples. Ö.K. wishes to thank Professor Rui Rui Du, Dr. Kristjan Stone, and Dr. Zhouquan Yuan of Rice University, Department of Physics and Astronomy for their valuable discussions and suggestions during ^{3}He insert installations. Ö.K. wishes to thank Muharrem Demir from NanoMagnetics Instruments for his support during manufacturing processes.

[1] G. Binnig, C. F. Quate, and Ch. Gerber, Phys. Rev. Lett. **56**, 930 (1986).
[2] Y. Martin and H. K. Wickramasinghe, Appl. Phys. Lett. **50**, 1455 (1987).
[3] A. Moser, H. J. Hug, I. Parashikov, B. Stiefel, O. Fritz, H. Thomas, A. Baratoff, H. J. Güntherodt, and P. Chaudhari, Phys. Rev. Lett. **74**, 1847 (1995).
[4] A. Volodin, K. Temst, A. Van Haesendonck, Y. Bruynseraede, M. I. Montero, and I. K. Schuller, Europhys. Lett. **58**, 582 (2002).
[5] A. Schwarz, U. H. Pi, M. Liebmann, R. Wiesendanger, Z. G. Khim, and D. H. Kim, Appl. Phys. Lett. **88**, 012507 (2006).
[6] M. Roseman and P. Grütter, J. Appl. Phys. **91**, 8840 (2002).
[7] U. H. Pi, A. Schwarz, M. Liebmann, R. Wiesendanger, Z. G. Khim, and D. H. Kim, Phys. Rev. B **73**, 144505 (2006).
[8] L. Luan, O. M. Auslaender, D. A. Bonn, R. Liang, W. N. Hardy, and K. A. Moler, Phys. Rev. B **79**, 214530 (2009).
[9] E. W. J. Straver, J. E. Hoffman, O. M. Auslaender, D. Rugar, and K. A. Moler, Appl. Phys. Lett. **93**, 172514 (2008).
[10] W. Wu, C. Israel, N. Hur, S. Park, S. W. Cheong, and A. de Lozanne, Nat. Mater. **5**, 881 (2006).
[11] A. Lakhani, P. Kushwaha, R. Rawat, and P. Chaddah, Appl. Surf. Sci. **256**, 404 (2009).
[12] A. Schwarz, M. Liebmann, U. Kaiser, R. Wiesendanger, T. W. Noh, and D. W. Kim, Phys. Rev. Lett. **92**, 077206 (2004).

[13]M. Liebmann, A. Schwarz, U. Kaiser, R. Wiesendanger, D.-W. Kim, and T. W. Noh, Phys. Rev. B **71**, 104431 (2005).
[14]L. Landau, J. W. Reiner, and L. Klein, J. Appl. Phys. **111**, 07B901 (2012).
[15]P. Milde *et al.*, Science **340**, 1076 (2013).
[16]U. Hartmann, Annu. Rev. Mater. Sci. **29**, 53 (1999).
[17]A. de Lozanne, Microsc. Res. Tech. **69**, 550 (2006).
[18]A. Schwarz and R. Wiesendanger, Nano Today **3**, 28 (2008).
[19]H. J. Hug, Th. Jung, and H.-J. Güntherodt, Rev. Sci. Instrum. **63**, 3900 (1992).
[20]R. Euler, U. Memmert, and U. Hartmann, Rev. Sci. Instrum. **68**, 1776 (1997).
[21]M. Roseman and P. Grütter, Rev. Sci. Instrum. **71**, 3782 (2000).
[22]E. Straver, Ph.d. thesis, Stanford University, 2004.
[23]T.-M. Chuang and A. L. de Lozanne, Rev. Sci. Instrum. **78**, 053710 (2007).
[24]M. Liebmann, A. Schwarz, S. M. Langkat, and R. Wiesendanger, Rev. Sci. Instrum. **73**, 3508 (2002).
[25]C. W. Yuan, E. Batalla, M. Zacher, A. L. de Lozanne, M. D. Kirk, and M. Tortonese, Appl. Phys. Lett. **65**(10), 1308 (1994).
[26]Y. Seo, P. C. Zimansky, and V. Chandrasekhar, Appl. Phys. Lett. **87**, 103103 (2005).
[27]E. Nazaretski, K. S. Graham, J. D. Thompson, J. A. Wright, D. V. Pelekhov, P. C. Hammel, and R. Movshovich, Rev. Sci. Instrum. **80**, 083704 (2009).
[28]D. V. Pelekhov, J. B. Becker, and G. Nunes, Jr., Rev. Sci. Instrum. **70**, 114 (1999).
[29]Nanosensors Inc., Rue Jaquet- Droz 1, Case Postale 216, CH-2002, Neuchatel, Switzerland.
[30]Applied NanoStructures Inc., 415 Clyde Ave, Suite 102, Mountain View, CA 94043, U.S.A.
[31]D. Rugar, H. J. Mamin, and P. Guethner, Appl. Phys. Lett. **55**(25), 2588 (1989).
[32]A. Oral, R. A. Grimble, H. Ö. Özer, and J. B. Pethica, Rev. Sci. Instrum. **74**, 3656 (2003).
[33]T. Fukuma and S. P. Jarvis, Rev. Sci. Instrum. **77**, 043701 (2006).
[34]Q. Zhong, D. Innis, K. Kjoller, and V. B. Ellings, Surf. Sci. **290**, L688 (1993).
[35]H. I. Rasool, P. R. Wilkinson, A. Z. Stieg, and J. K. Gimzewski, Rev. Sci. Instrum. **81**, 023703 (2010).
[36]B. W. Hoogenboom, P. L. T. M. Frederix, J. L. Yang, S. Martin, Y. Pellmont, M. Steinacher, S. Zäch, E. Lagenbach, H.-J. Heimbeck, A. Engel, and H. J. Hug, Appl. Phys. Lett. **86**, 074101 (2005).
[37]See www.nanomagnetics-inst.com for NanoMagnetics Instruments Ltd., Oxford, U.K.